Available online at www.sciencedirect.com
ScienceDirect
Polymer 48 (2007) 5626–5638
polymer
www.elsevier.com/locate/polymer

Orientation relaxation study on poly(ethylene oxide)–poly(vinyl phenol) blends by polarization modulation infrared linear dichroism

François Lapointe, Michel Pézolet, Josée Brisson*

Centre de recherche en science et ingénierie des macromolécules (CERSIM), Département de chimie, Faculté des sciences et de génie, Université Laval, Québec, Canada G1K 7P4

Received 15 June 2007; received in revised form 13 July 2007; accepted 16 July 2007
Available online 20 July 2007

Abstract

Orientation relaxation in miscible poly(vinyl phenol) (PVPh)–poly(ethylene oxide) (PEO) blends (from 25 to 40 wt% PEO) was investigated using polarization modulation infrared linear dichroism. This blend was selected to study the effect of strong hydrogen bonds on relaxation. The results show that PEO is more oriented than PVPh, and remains so throughout the experimental relaxation time. Relaxation proceeds in three stages. PVPh relaxation is systematically faster than that of PEO, while PEO relaxation times increase steadily with increasing PEO content. For PVPh, a maximum in relaxation times is observed around 30 wt% PEO. Relaxation coupling occurs for concentrations in PEO lower than 30 wt%, is marginal for the 35 wt% and clearly absent for the 40 wt% PEO blend. By comparison with previous rheology and near-infrared data, it can be concluded that hydrogen bonds do not automatically insure cooperativity during relaxation: for cooperativity to occur, the minor component of the blend must interact preferentially with the major component. This is the case of PVPh-rich compositions, but not for PEO-rich compositions (for 35 and 40 wt% PEO), for which the minor PVPh constituent interacts strongly with both PEO and other PVPh chains.

Keywords: Poly(vinyl phenol); Orientation; Poly(ethylene oxide)

1. Introduction

Miscible amorphous polymer blends behave in most respects like homopolymers. A single phase is observed in microscopy, they do not diffuse light, a single T_g is observed in thermal analysis, and mechanical properties are generally intermediate between those of the homopolymers they contain. However, chains of each component may react differently to an applied stress. Orientation and relaxation measurements often show significant differences in the behavior of the two types of chains, despite the fact that they belong to the same phase [1].

It is generally agreed upon that relaxation is influenced by interchain interactions, which are mathematically expressed by changes in friction coefficient, as well as chain entanglements. The most widely accepted model to account for relaxation in polymer dynamics has been proposed by Doi and Edwards. In this model, relaxation proceeds in three steps: Rouse-like relaxation between entanglement points, related to a first relaxation time τ_e, a retraction of chain ends inside the tube, related to τ_R, and finally reptation outside of the tube, first proposed by de Gennes [2], with an associated relaxation time τ_d. Surprisingly, however, the behavior of hydrogen bond forming blends has not been easy to rationalize. In some instances, hydrogen bonds were found to increase orientation [3], in others they were found to have no detectable effect [3,4].

Our group has focused on the orientation of poly(vinyl phenol) (PVPh)-containing blends, which were found to have unexpected orientation behaviors, such as a maximum

* Corresponding author. Tel.: +1 (418) 656 3536; fax: +1 (418) 656 7916.
E-mail addresses: francois.lapointe@chm.ulaval.ca (F. Lapointe), michel.pezolet@chm.ulaval.ca (M. Pézolet), josee.brisson@chm.ulaval.ca (J. Brisson).

0032-3861/$ - see front matter © 2007 Elsevier Ltd. All rights reserved.
doi:10.1016/j.polymer.2007.07.034

in orientation in two different systems, tentatively linked to the formation of hydrogen bonds [5–8]. Quantification of orientation in previous PVPh-based work was, however, challenging, as relaxation itself is difficult to separate from initial orientation induced by the deformation process. Orientation measurements of various components in a blend are possible using infrared spectroscopy techniques, but are often complicated by band overlap. Determining the angle between the transition moment of the vibration and the chain axis, which is mandatory for quantitative chain orientation determination, is often a problem in itself [1].

The introduction of polarization modulation infrared dichroism (PM-IRLD) has improved markedly the sensitivity and time scale for orientation measurement of orientation as the dichroic difference (ΔA) is measured directly [9]. The dichroic difference ΔA can be used to compute the Hermans orientation factor observed at time t, $\langle P_2(\cos\theta, t)\rangle$, using the following equation:

$$\langle P_2(cos\,\theta,t)\rangle = \frac{2}{3cos^2\,\alpha - 1}\frac{\sqrt{\lambda}}{3A_0}\quad \Delta A(t) \tag{1}$$

where λ is the draw ratio, α the angle between the chain axis and the transition dipole moment of the vibration, and A_0 the absorbance of a band in an isotropic sample at time zero (before stretching). It has been shown that this method yields orientation measurements comparable, for homopolymers, to those obtained by birefringence [10,11]. PM-IRLD has further been used to investigate the orientation behavior of copolymers [12] and blends [13,14].

In the present work, PM-IRLD has been used to revisit a previously studied hydrogen bond forming blend, poly(vinyl phenol) (PVPh)–poly(ethylene oxide) (PEO) [6]. This blend is well known to form strong hydrogen bonds [15] and to be homogeneous down to at least the 20 nm scale, as evidenced by differential scanning calorimetry (DSC) [16] and NMR measurements [17,18]. PM-IRLD allows measurements of orientation changes after deformation. Furthermore, the time elapsed between the measurements and the end of the deformation is much smaller than when performing sample quenching prior to static orientation measurements (approximately 0.5 s, as compared to a few seconds). It can therefore allow a better understanding of this system and the influence that hydrogen bonds have on its orientation and relaxation behavior.

2. Experimental section

2.1. Sample preparation and characterization

PEO was purchased from Aldrich Chemical Company, whereas PVPh was obtained from ChemFirst Inc. Gel permeation chromatography was performed on both polymers with HPLC-grade chloroform (PEO) or THF (PVPh) using a Dawn DSP size exclusion chromatograph equipped with a Rheodyne 715 injector, a Waters HPLC 515 pump and an Optilab 903 refractive index detector from Wyatt. For PEO, a Shodex KF-804 column and an Ultrastyragel linear column were used, while for PVPh, only the KF-804 column was used. Measurements were performed at 25 °C, and reported molecular weights were established using polystyrene (PS) standards. For PEO, a M_w of 830,000 g mol^{-1} and I_p of 1.60 were measured for the polymer used in most experiments, whereas, when specified, a polymer with M_w of 430,000 g mol^{-1} and I_p of 1.52 was used. For PVPh, measurements were performed using a polymer with M_w of 32,800 g mol^{-1} and I_p of 1.28.

Differential scanning calorimetry was performed using a Perkin–Elmer DSC-7 equipped with a CCA-7 cooling module, calibrated with indium. Reported endpoint T_{gf} was obtained at the second scan and was determined as the intersection of the tangent of the curves during and after the glass transition. In some cases, glass transition is also reported as T_g, the midpoint of the two tangents before and after the transition or the onset, T_{gi}, which corresponds to the intersection of the tangents of the curves before and during the transition. Crystallinity was determined as being zero, within experimental error, from the absence of a melt endotherm in differential scanning calorimetry.

Solutions of the two polymers were prepared at 60 °C under nitrogen atmosphere, using benzyl alcohol as the solvent, at a concentration of one gram of polymer blend per 10 mL benzyl alcohol. The mixture was stirred for 12 h using a mechanical mixer.

Films were prepared by solution casting on a HDPE surface and the solvent was evaporated under a fume hood for a week. Films were then removed from the HDPE support and placed in a vacuum oven for a week at room temperature. Subsequent drying was achieved by raising the temperature by 10 °C steps each day until a temperature of $T_g + 15$ °C was reached for the specific blend composition. Films were then allowed to dry further for 3 weeks in the oven. Resulting films were free of bubbles and had reached a constant T_g. Final transition temperatures T_g, T_{gi} and T_{gf} are reported in Table 1. Films were kept under vacuum in a desiccator until used.

Thinner films were required for infrared spectroscopy. These were obtained by applying a pressure of 10 metric tons for 5 min at a temperature of $T_g + 55$ °C using a Carver press. The process was repeated until a thickness of 20–30 μm was reached. Samples were then inserted in a vacuum oven for 2 h at a temperature of $T_{gf} + 20$ °C to remove residual stress, and the absence of initial orientation was verified by static Fourier transform infrared spectroscopy (FTIR) linear

Table 1
PVPh–PEO blend characterization ($M_w^{PEO} = 830{,}000$ g mol^{-1})

Blend composition (PEO, wt%)	Blend composition (PEO, mol%)	T_g (°C)	T_{gi} (°C)	T_{gf} (°C)	Crystallinity (%)
0	0	186 ± 2	182 ± 2	190 ± 2	0
20	40	113 ± 2	103 ± 2	121 ± 2	0
25	48	103 ± 3	93 ± 2	111 ± 6	0
30	54	85 ± 1	76 ± 1	92 ± 1	0
35	59	61 ± 2	52 ± 2	69 ± 1	0
40	65	53 ± 1	44 ± 1	62 ± 2	0
100	100	−58 ± 1	−63 ± 1	−54 ± 1	40

dichroism measurements. Samples were cut to dimensions of 7 mm × 30 mm and each end was covered with Pyrotape (Aremco Inc.) before being inserted in the stretcher.

2.2. FTIR characterization

FTIR spectra of pure polymer and blend films were measured at a 4 cm^{-1} resolution using a Nicolet Magna 560 FTIR spectrometer equipped with a liquid nitrogen cooled MCT detector. For each sample, 200 scans were recorded. PM-IRLD measurements were performed using a Bomem MB-100 FTIR spectrometer equipped with a Globar IR source. Infrared polarization was modulated using a photoelastic modulator PEM-90 from Hinds consisting of a ZnSe crystal with a natural frequency of 50 kHz coupled to a pair of piezoelectric transducers. The photoelastic modulator was optimized for 3020 cm^{-1}, and the retardation was set to $\lambda/2$. The experimental setup used for PM-IRLD has been described in more details in previous references [9,19]. A custom-made mechanical stretcher was used to allow recording of spectra during deformation and relaxation at a given temperature. Samples were stretched at a 0.158 cm s^{-1} speed using a 1000 steps s^{-2} acceleration to a draw ratio of $\lambda = 1.5$, followed by a 12,000 steps s^{-2} deceleration at temperatures ranging from $T_{gf} + 2$ to $T_{gf} + 10$ °C.

Spectra were acquired in three steps during the relaxation period: During the first 288 s, 180 spectra consisting of 4 scans each were recorded, as this was the portion where the best time resolution was sought. In the subsequent 1080 s, 90 spectra of 30 scans each were averaged, and in the final step, where orientation was low and therefore the need to optimize signal-to-noise ratio was greater, 80 spectra of 75 scans each were recorded. In all cases, sample thickness was adjusted in order to maintain the absorbance of the two bands of interest (951 and 3021 cm^{-1}) below 0.8 to work in the domain where the response of the detector is linear. The two bands selected to follow relaxation lie far from one another and, therefore, are not situated on the same modulation arch. The photoelastic modulator was adjusted to optimize the 3020 cm^{-1} PVPh band. Because the chosen PEO band lies close to the maximum of a different arch, error introduced by the vibration choice should be minimal.

Averaged relaxation curves, obtained using at least three different experimental curves, were used for calculations. Reported errors correspond to the Student test with a 95% probability, unless otherwise stated. Spectral treatment was performed using Galactic Instruments GRAMS/AI version 7.0. Non-linear regression of relaxation curves were performed using the Microlab Origin 6.0 software.

3. Results and discussion

3.1. Miscibility

PEO–PVPh blend preparation was performed by solution evaporation. Benzyl alcohol was used because of its slow evaporation which yielded high quality films, in spite of the fact that this required long evaporation times, due to the low vapor pressure of the solvent and to the gradual heating scheme used, which yielded bubble-free films. DSC thermograms of PVPh–PEO blend are reported in Fig. 1. As can be seen, in the temperature range reported, a single glass transition is observed, the glass transition temperature varies monotonously with composition, and no significant transition broadening occurs. This clearly indicates that, if microphase separation is present, it is well below the detection limits of the DSC technique, which is approximately of 2–15 nm [20]. Reference temperatures are reported as $T_{gf} + x$ °C, the endpoint T_{gf} being listed in Table 1, as mentioned previously.

3.2. Band selection for orientation measurements

FTIR spectra of blends of different compositions in two regions of interest are shown in Fig. 2. For the PEO characterization, the band at 951 cm^{-1} (Fig. 2a), due to the antisymmetric rocking of the CH_2 *gauche* segments, coupled with C–C stretching vibration, was used as in a previous study of the PVPh–PEO blend [6]. A 48° value was used for the α angle of this vibration [6]. For PVPh characterization, the 3021 cm^{-1} (Fig. 2b) aromatic ring C–H elongation band was selected. The α angle for this band was proposed to be close to 90° [21]. In this region are also located the broad O–H elongation vibration band centered around 3500 cm^{-1}, and the aliphatic C–H stretching vibration below 3000 cm^{-1}. The O–H band can be separated into various components (non-bonded or free hydroxyl groups, hydroxyl groups involved in PVPh–PVPh hydrogen bonds or intrachain interactions and hydroxyl groups involved in PVPh–PEO hydrogen bonds or interchain interactions), as was performed in a previous work to determine the proportion of hydrogen bonds of each type in the blends [22].

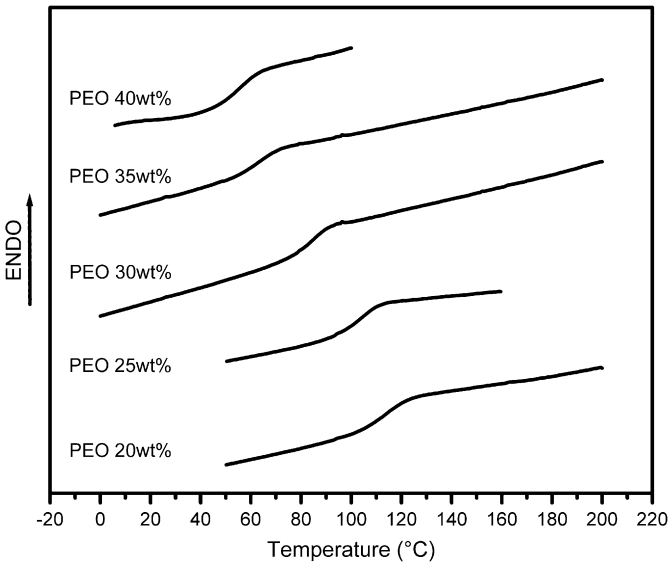

Fig. 1. DSC thermograms of PEO–PVPh blends.

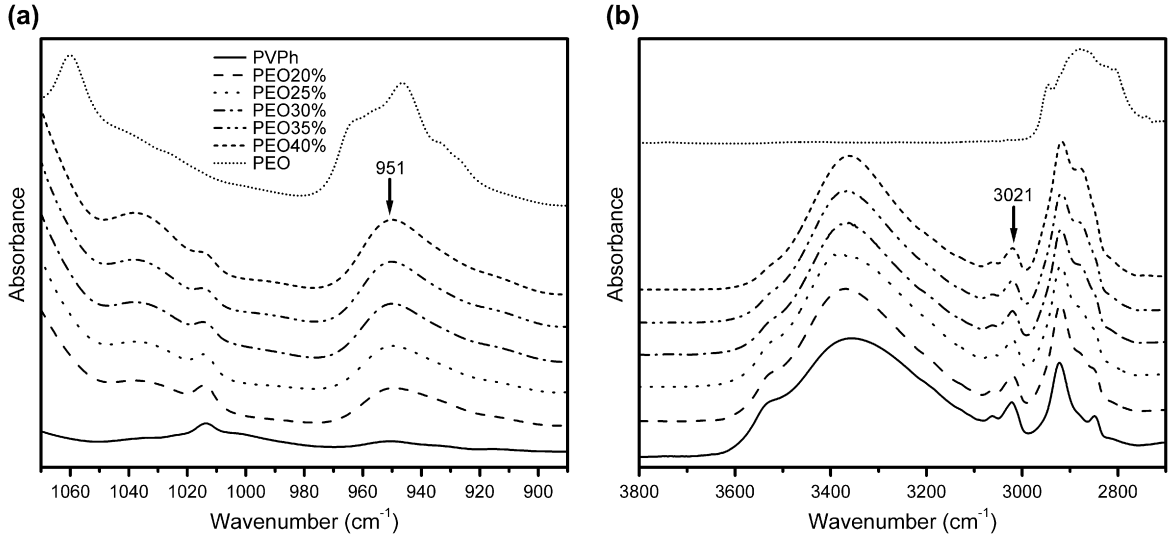

Fig. 2. FTIR spectra of PEO–PVPh blends: (a) 1070–880 cm^{-1} region, (b) 4000–2000 cm^{-1} region.

3.3. PM-IRLD measurements of orientation and subsequent deformation

Fig. 3 shows typical dichroic difference spectra ΔA in the two regions of interest during the post-deformation relaxation period. As can be seen, the dichroic difference peak decreases in intensity with time. The most striking difference between the two investigated bands is the fact that the ΔA peak is positive for the PEO band whereas it is negative for the PVPh band. This is in agreement with the fact that the α angle of each component is on different sides of the magic angle (54.7° for the second moment of the Legendre polynomial, $P_2(\cos\theta)$), with an α angle of 48° for the PEO 951 cm^{-1} band, whereas the α angle is 90° for the PVPh 3021 cm^{-1} band. Therefore, the transition moment associated with the PEO band is more parallel to the deformation direction, whereas that of the PVPh band is perpendicular. A second difference lies in the noise level that is much larger for the 3021 cm^{-1} band. This is mainly due to the lower orientation of PVPh, and to background instabilities during the dynamical experiment, related to the proximity of high intensity bands (ν OH and aliphatic ν CH). Relaxation curves of PVPh will therefore be determined with less accuracy than for PEO. Finally, after approximately 4000 s, whereas a residual ΔA peak can be seen for the PEO band, in the case of PVPh, orientation appears to be completely lost, and no dichroic difference peaks remain in the 3021 cm^{-1} region.

From the observed dichroic difference, the orientation factor $\langle P_2(\cos\theta)\rangle$ can be determined. Fig. 4 shows the relaxation behavior of both PVPh and PEO for a representative 30 wt% PEO sample. As can be seen, PVPh orientation converges to a value close to zero after approximately 500 s, whereas

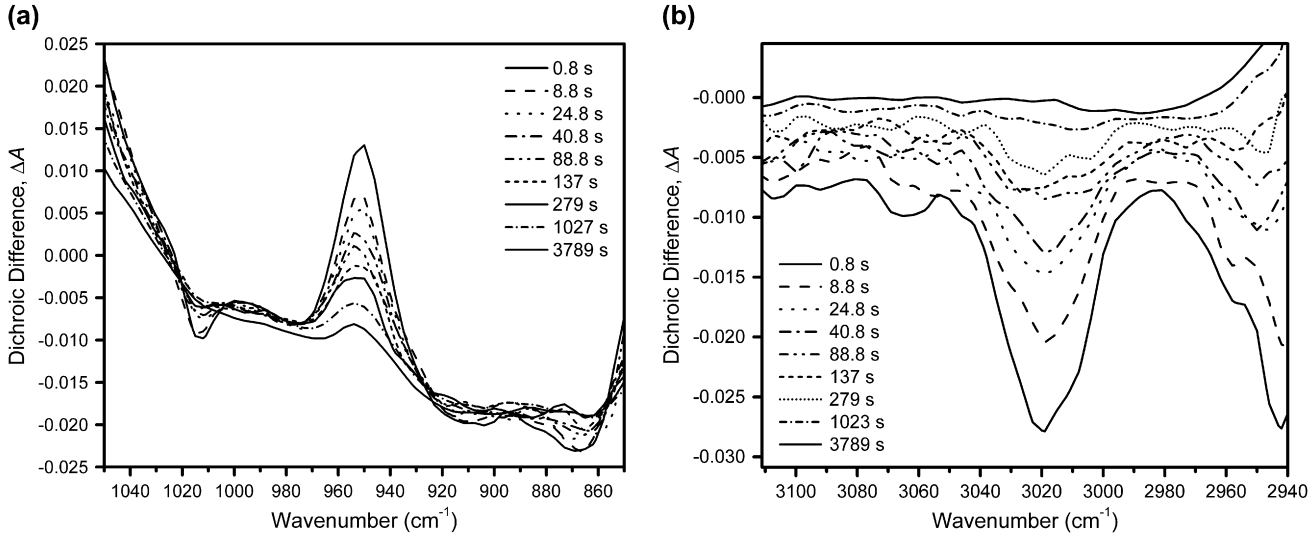

Fig. 3. PM-IRLD dichroic difference spectra of a representative 30% PEO sample at various times after deformation: (a) 951 cm^{-1} PEO band, (b) 3021 cm^{-1} PVPh band.

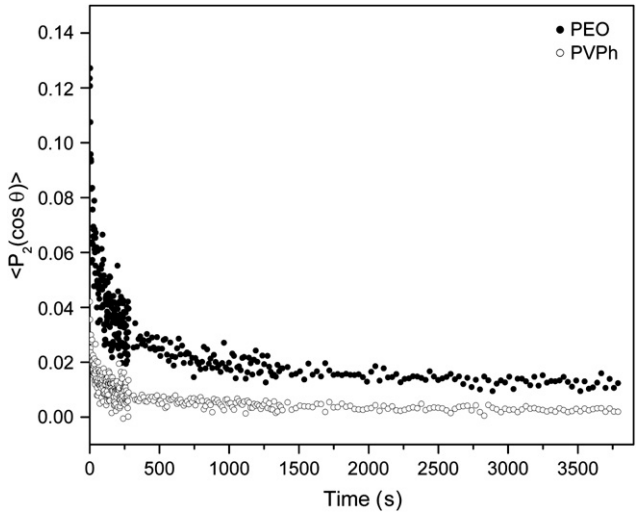

Fig. 4. Average orientation relaxation curves of PVPh and PEO in a 30 wt% PEO blend ($\lambda = 1.5$, $T = T_{gf} + 2\ ^{\circ}C$, $M_w^{PEO} = 830{,}000\ g\ mol^{-1}$).

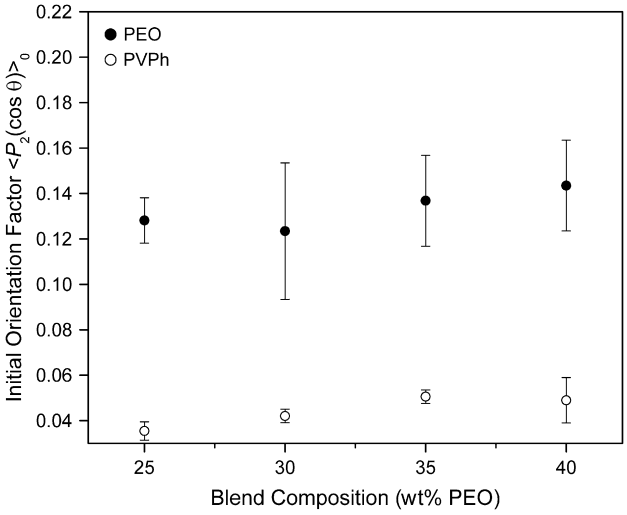

Fig. 5. Initial orientation factor $\langle P_2(\cos\theta)\rangle_o$ observed immediately after stretching, at time $t = 0.8$ s, for various PVPh–PEO blends ($\lambda = 1.5$, $T = T_{gf} + 2\ ^{\circ}C$, $M_w^{PEO} = 830{,}000\ g\ mol^{-1}$).

PEO remains oriented throughout the experiment, as previously observed in Fig. 3. The sudden decrease in data dispersion around 300 s is associated with the change in data acquisition regime, which changes from 4 scans per spectra during the first 300 s of the relaxation process, when orientation decreases steadily, to 30 scans per spectra when these changes slow down. This was used to optimize relaxation time determination from these curves: a higher number of scans right after elongation, when relaxation is at its fastest, would have resulted in a loss in time resolution where most needed, whereas a smaller number of scans at higher times increases experimental error without any notable gain in time resolution, variations being much slower at this point. However, these experimental conditions improve accuracy of relaxation time determination at the cost of a loss in $\langle P_2(\cos\theta)\rangle$ precision during the first 300 s of the experiment.

In Fig. 5 is reported the orientation factor $\langle P_2(\cos\theta)\rangle_0$ measured immediately after stretching, at time 0.8 s, which corresponds to the end of the first spectra taken. This is the point where measured orientation is highest, since relaxation is the most limited. In each case, values reported were estimated using 3–7 different samples. As can be seen, error bars are larger for PEO, in spite of the fact that intensity of the band used is larger for this polymer. This is related to the value of the α angle, which is of 48° for the PEO band, a value close to the magic angle of 54.7°. In this context, a small change in dichroic difference from one sample to another yields a large change in the orientation factor, hence increasing the error on $\langle P_2(\cos\theta)\rangle$. However, when following the relaxation of a given sample, the error will be much lower for PEO, as the α angle will cause a systematic error on the successive $\langle P_2(\cos\theta)\rangle$ values of the sample, but will not affect the relaxation times which are derived from the curves.

One of the salient features of Fig. 5 is that, at the beginning of relaxation, orientation values are systematically larger by a factor of 2–3 for PEO than for PVPh. It must be noted that the PEO band used is that of *gauche* segments, such as those appearing in the helical conformation adopted by the chain in its crystalline state. The reported orientation factor therefore pertains solely to these segments of the blend.

For PEO, no $\langle P_2(\cos\theta)\rangle_0$ variation with composition is observable within the experimental error. For comparison purposes, orientation values of the PEO–PVPh system previously reported by Rinderknecht and Brisson [6], using conventional FTIR dichroism on samples quenched after stretching for a small elongation ratio ($\lambda = 1.5$), varied from 0.05 to 0.07, and that a maximum in orientation was observed for the 30 wt% PEO composition, which is not the case here. Important differences exist between the two different studies, including first and foremost the time elapsed between deformation and measurement, but also polymer molecular weights. In the present case, PVPh molecular weight is slightly above the molecular weight between entanglements M_e (32,800 g mol^{-1} vs 29,300 g mol^{-1} [23]), whereas in the original work by Rinderknecht and Brisson, it was much closer to the molecular weight between entanglements of PEO than that of PVPh (5200 g mol^{-1} vs 2200 g mol^{-1} [24] for M_e of PEO, and 29,300 g mol^{-1} [23] for M_e of PVPh), and was therefore probably marginally entangled at best. In addition, a tenfold difference existed between the molecular weights of PEO in both studies (82,500 g mol^{-1} in the work by Rinderknecht and Brisson, 830,000 g mol^{-1} in the present work).

In the case of PVPh, orientation generally increases with PEO content in the composition range studied. Only two compositions of PEO–PVPh blends had been studied by Rinderknecht and Brisson [6]. $\langle P_2(\cos\theta)\rangle$ values reported in this first study, which varied from 0.01 to 0.03 for at $\lambda = 1.5$, are slightly lower than in the present case, again as expected from the use of lower molecular weight PEO and PVPh. Therefore, within experimental error, and considering the differences in molecular weights used, both studies generally show a good agreement in orientation values both for PEO and PVPh.

Relaxation changes can be visualized in Fig. 6, which shows the relaxation curves for the four blends studied on a semi-logarithmic time scale. Straight lines have been superimposed as visual guidelines to highlight the different regions of the curves. As can be seen, the curves are not linear over the entire time range, and a single relaxation time is not sufficient to explain these curves, as predicted by the Doi–Edwards relaxation model and as observed previously for homopolymers and miscible polymer blends [25–27].

3.4. Quantification of relaxation times for the PVPh–PEO blends

Various methods have been proposed to extract the characteristic relaxation times from relaxation curves. Tassin and Monnerie [28] have proposed the following equation to link $\langle P_2(\cos\theta)\rangle$ to the Doi–Edwards theory:

$$\langle P_2(cos\,\theta,t)\rangle = \frac{\langle P_2(cos\,\theta)\rangle^{\text{network}}}{\alpha^2(\lambda)}\left[1+\sum_{p=1}^{N_e} exp\left(\frac{-tp^2}{\tau_e}\right)\right] \times\left[1+(\alpha(\lambda)-1)\sum_{p\ \text{odd}}\frac{8}{p^2\pi^2}exp\left(\frac{-tp^2}{\tau_R}\right)\right]^2\sum_{p\ \text{odd}}\frac{8}{p^2\pi^2}exp\left(\frac{-tp^2}{\tau_d}\right) \quad (2)$$

where $\langle P_2(\cos\theta)\rangle^{\text{network}}$ is the orientation at the end of the first relaxation process, $\alpha(\lambda)$ is the microscopic deformation ratio of the primitive segments and τ_e, τ_R, τ_d are the relaxation times. In practice, as the first term of each summation is the one which contributes the most, only the $p=1$ term is used. The $\alpha(\lambda)$ is usually calculated from the affine model using the following equation derived from the Gaussian rubber theory [29]:

$$\alpha(\lambda) = \frac{1}{2}\left(\lambda + \frac{sinh^{-1}x}{x\lambda^{1/2}}\right) \quad (3)$$

where $x = (\lambda^3-1)^{1/2}$.

The following third-order exponential decay function can also be used to fit relaxation data:

$$\langle P_2(cos\,\theta,t)\rangle = A_1\,exp\left(\frac{-t}{\tau_1}\right)+A_2\,exp\left(\frac{-t}{\tau_2}\right)+A_3\,exp\left(\frac{-t}{\tau_3}\right) \quad (4)$$

where A_1, A_2, A_3 are exponential prefactors. This equation has recently been used for relaxation characterization of PM-IRLD data [11].

Eqs. (2) and (4) have both been used in the present work. In the case of the Tassin–Monnerie equation, fits were first made by fixing the value of $\alpha(\lambda)$ to that calculated using Eq. (3), using only four variables, τ_e, τ_R, τ_d and $\langle P_2(\cos\theta)\rangle^{\text{network}}$. However, as seen in Fig. 7, which reports typical curve fittings, this did not result in reasonable fits for all compositions. A second series of fits was therefore performed using $\alpha(\lambda)$ as a fifth variable. This provided, as seen in Fig. 7, satisfactory fits with experimental data. Equally satisfactory and almost perfectly superimposable fits were obtained using the third-order exponential decay function as was previously the case for other homopolymers and polymer blends studied by PM-IRLD [11,25–27]. Attempts were also made to fit the data using Eq. (4) and a smaller number of relaxation times, without success.

To emphasize the fact that it is a fit of experimental data, in the rest of the discussion, τ_e, τ_R, τ_d will be replaced by characteristic relaxation times τ_1, τ_2, τ_3. Furthermore, relaxation values obtained by the Tassin–Monnerie equation are discussed in more detail for three main reasons. Firstly, this method uses a lower number of fitting parameters (five in the present case, three τ values, $\alpha(\lambda)$ and $\langle P_2(\cos\theta)\rangle^{\text{network}}$, as compared to six for the other method). Secondly, Tassin and Monnerie have proposed a physical significance for all of these fitting variables, which is not the case in the second method. Finally, as opposed to a third-order exponential decay, the Tassin–Monnerie equation takes into consideration the fact that the term related to retraction should be elevated to

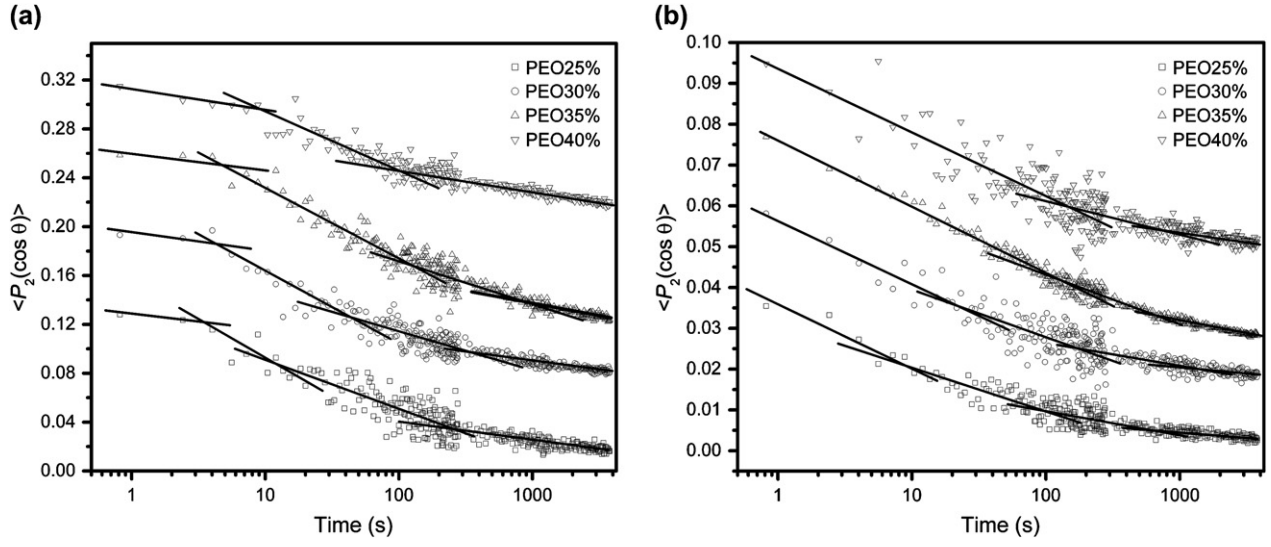

Fig. 6. Averaged relaxation curves of the two polymers in the PEO–PVPh blends ($\lambda = 1.5$, $T = T_{gf} + 2$ °C, $M_w^{PEO} = 830{,}000$ g mol^{-1}). Data shifted along the y axis for clarity purposes, y scale pertains to data for the PEO 25% composition. (a) PEO, (b) PVPh.

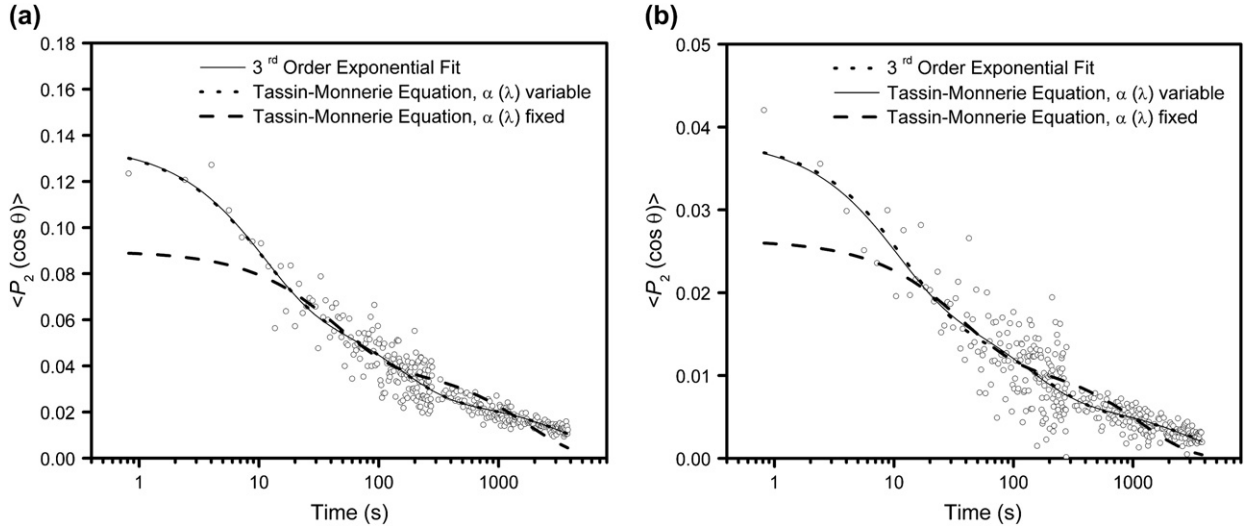

Fig. 7. Typical curve fitting using a third-order exponential decay and the Tassin–Monnerie equation for a 30 wt% PEO blend ($\lambda = 1.5$, $T = T_{gf} + 2\,^{\circ}C$, $M_w^{PEO} = 830{,}000\ g\ mol^{-1}$): (a) PEO, (b) PVPh.

the power of 2 to follow the expression of anisotropic stress between τ_e and τ_R, as stipulated in Doi–Edwards theory [30].

The main problem with this choice lies in the use of a variable $\alpha(\lambda)$ value. This indicates that, contrary to predictions using the rubber theory, deformation is not affine at the molecular scale. As can be seen in Fig. 8, for PVPh, both the $\alpha(\lambda)$ and $\langle P_2(\cos\theta)\rangle^{network}$ values remain, within experimental error, relatively constant, which indicates that this approximation is valid. For PEO, however, a marked decrease in $\alpha(\lambda)$ occurs for 30 and 40 wt% PEO, which indicates a deviation from the affine model. Takahashi et al. [31], when studying pure, semi-crystalline PEO, previously observed that PEO does not follow an affine deformation model, even in the crystalline phase. This was attributed to changes in conformation of PEO upon deformation, leading to increase in the length of the repeat unit. In the present case, for low PEO concentrations, the $\alpha(\lambda)$ value remains constant and, therefore, the affine model is followed to a first approximation. This may be due to the formation of strong interactions with PVPh, rigidifying the chains and therefore decreasing conformation changes which lead to non-affine behavior. On the other hand, at higher PEO concentrations, the system resumes its normal non-affine behavior and the $\alpha(\lambda)$ consequently decrease substantially.

Relaxation times τ determined using the Tassin–Monnerie equation and third-order exponential decay function are reported in Table 2 for different blend compositions. Relaxation times obtained from these two approaches are generally

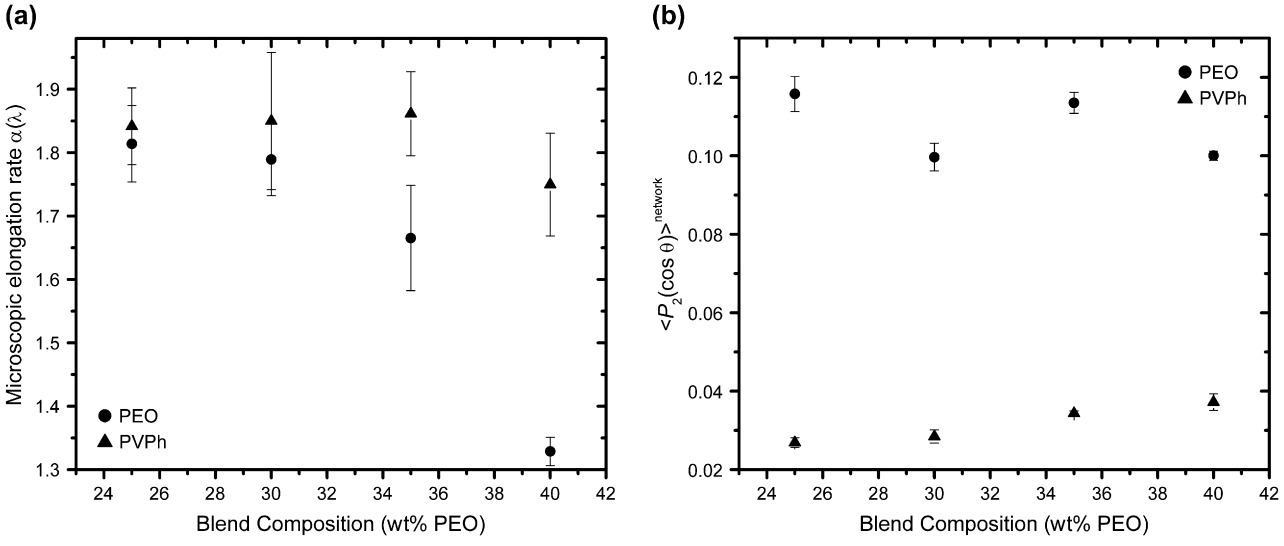

Fig. 8. Values obtained for adjustable parameters in the Tassin–Monnerie fits as a function of blend composition ($\lambda = 1.5$, $T = T_{gf} + 2\,^{\circ}C$, $M_w^{PEO} = 830{,}000\ g\ mol^{-1}$). (a) $\alpha(\lambda)$, (b) $\langle P_2(\cos\theta)\rangle^{network}$.

Table 2
Relaxation times and fitting parameters ($\lambda = 1.5$, $T = T_{gf} + 2$ °C, $M_w^{PEO} = 830{,}000$ g mol^{-1})

	PEO 25%		PEO 30%		PEO 35%		PEO 40%	
	PEO	PVPh	PEO	PVPh	PEO	PVPh	PEO	PVPh
(a) Calculated using the Tassin–Monnerie equation								
τ_1 (s)	6 ± 1	6 ± 1	10 ± 2	10 ± 3	27 ± 2	20 ± 1	31 ± 2	9 ± 2
τ_2 (s)	160 ± 20	120 ± 10	160 ± 20	150 ± 30	430 ± 60	260 ± 20	1300 ± 200	150 ± 20
τ_3 (s)	7000 ± 1000	4000 ± 600	4300 ± 600	3100 ± 700	7000 ± 2000	2400 ± 200	1e21	5000 ± 1000
$P_2^{network}$	0.116 ± 0.005	0.027 ± 0.001	0.100 ± 0.004	0.028 ± 0.002	0.113 ± 0.003	$3.43E-2 \pm 6E-4$	0.100 ± 0.00	0.037 ± 0.002
$\alpha(\lambda)$	1.81 ± 0.06	1.84 ± 0.06	1.79 ± 0.07	1.8 ± 0.1	1.66 ± 0.08	1.86 ± 0.07	1.33 ± 0.02	1.75 ± 0.08
R^2	0.844	0.858	0.908	0.798	0.941	0.977	0.908	0.786
(b) Calculated using the third-order exponential decay function								
τ_1 (s)	8 ± 2	6 ± 1	10 ± 1	12 ± 2	23 ± 3	17 ± 1	28 ± 3	9 ± 2
τ_2 (s)	110 ± 10	120 ± 10	140 ± 20	160 ± 30	270 ± 40	170 ± 10	300	110 ± 20
τ_3 (s)	6000 ± 1000	4300 ± 700	4300 ± 600	3500 ± 900	5400 ± 900	2800 ± 200	$14{,}000 \pm 2000$	4300 ± 1000
R^2	0.848	0.859	0.908	0.798	0.941	0.977	0.924	0.786

comparable within experimental error. For PEO, where obtained τ_3 values are above experimental times, fits were performed with missing end values and experimental error is consequently large. This is particularly true for the PEO 40 wt% τ_3 value, which yields an abnormally large value of 1×10^{21} s for the Tassin–Monnerie equation, and 14,000 s for the third-exponential decay function. This is due to orientation being virtually constant vs time at the end of the experiment. Therefore, this value will not be used in the following quantitative discussion. Longer acquisition times would have been necessary to better quantify this relaxation time but baseline instabilities prevented such measurements to be made.

Relaxation time evolution with respect to composition is reported in Fig. 9 for the Tassin–Monnerie approach. The first relaxation time for PEO increases steadily upon PEO blend content increase, whereas that of PVPh reaches a maximum at 35 wt% PEO content. The behavior of the second relaxation time is comparable, whereas for the third relaxation time, estimated errors are too large for any meaningful comparison to be made. The presence of such a maximum for PVPh is unexpected, and to our knowledge has never been observed previously.

3.5. Relaxation time attributions

The physical significance of the observed relaxation times is still the subject of debates. Messé and Prud'homme, using fits with a third-order exponential decay function, have proposed that the first relaxation time observed by PM-IRLD and birefringence is related to the τ_e Rouse-like relaxation time, and the third to the τ_R relaxation time of the Doi–Edwards model, whereas the second was tentatively attributed to relaxation of the chain ends [11]. These parameters are given, according to Doi–Edwards, by

$$\tau_e = \frac{\zeta N^2 b^2}{3\pi^2 k_B T Z^2}, \tag{5}$$

$$\tau_R = \frac{\zeta N^2 b^2}{3\pi^2 k_B T}, \tag{6}$$

$$\tau_d = \frac{\zeta N^2 b^2 Z}{\pi^2 k_B T}, \tag{7}$$

and

$$Z = M_w / M_e \tag{8}$$

where Z is the mean number of entanglements acting on a chain. Aside from temperature T, which is readily available, four variables are needed to estimate τ_e, τ_R and τ_d, and evaluate if the relaxation times observed experimentally can be assigned to these predicted relaxation modes: the number N and the length b of Rouse units forming the 'Rouse chain', the molecular mass between entanglements M_e and the chain friction coefficient ζ.

The length b of Rouse units can be assumed to be similar to that of Kuhn segments, and the value of b can be roughly estimated for each polymer from:

$$b = C_N b_0 \tag{9}$$

where C_N is the characteristic ratio and b_0 is the length of the repeat unit. Using previously published C_N values for pure PEO of 5.2 and for pure PVPh of 11.3 [32–34], Rouse unit length b is estimated as being around 1.4 nm for PEO and 2.8 nm for PVPh. A further approximation is to suppose that these values are constant with blend composition. The molecular weight between entanglements M_e has previously been reported for both pure polymers (2200 g for PEO [23] and 29,300 g for PVPh [24]). These are expected to vary upon blending, but should nevertheless be of the same order of magnitude as the value for the pure polymer. An estimation of the average chain friction coefficient in this blend has previously been made from rheology measurements, and yields a value of approximately 100 N s/m [8], which again, to a first approximation, can be taken as equal for both polymers.

From these values, Rouse-like relaxation times τ_e should be of the order of magnitude of 10 s for PEO and PVPh, and the

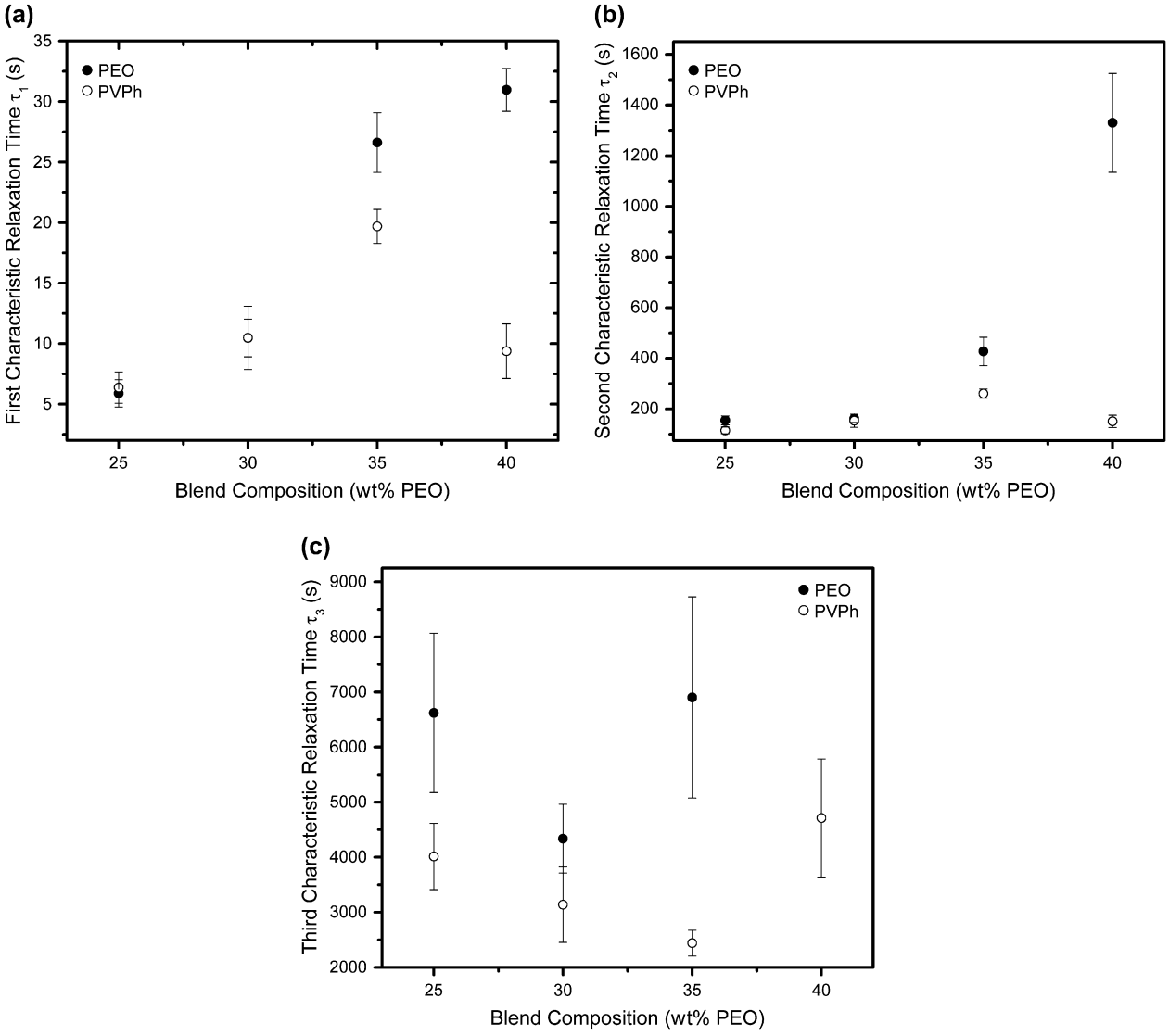

Fig. 9. Relaxation times calculated using the Tassin–Monnerie equation ($\lambda = 1.5$, $T = T_{gf} + 2\ ^\circ C$, $M_w^{PEO} = 830{,}000\ g\ mol^{-1}$). (a) First characteristic relaxation time, (b) second characteristic relaxation time, (c) third characteristic relaxation time.

retraction relaxation times of 100 s for PVPh and 10^6 s for PEO, whereas the reptation relaxation times should be of the order of 1000 s for PVPh and 10^8 s for PEO. Comparing with the estimated τ_e value of 10 s, the first characteristic relaxation time τ_1 observed in PM-IRLD of 6–31 s for PEO and 6–20 s for PVPh can be assigned to Rouse-like relaxation between entanglements (τ_e). This attribution is in agreement with previous PM-IRLD studies on various pure polymers and blends [13,14,27]. In previous PM-IRLD studies [13,26,27], the second characteristic relaxation time was left open or attributed tentatively to end-chain relaxation, and the third to retraction.

For PVPh, it is a safe assumption to correlate τ_2 and τ_3 with retraction and reptation processes, respectively, as ΔA decays to undetectable levels by the end of the experimental relaxation time, suggesting that orientation relaxation has been completed and reptation has occurred. Further, τ_2 varies from 120 to 260 s, of the same order of magnitude as the predicted 100 s value, whereas τ_3 varies from 2400 to 5000 s, and is of the same order of magnitude as the predicted 1000 s value.

For PEO, relaxation is clearly not finished at the end of the experimental times. Acquisition times over a longer period would not have given more information on the existence of additional relaxation times, as baseline instabilities would have affected data reliability. In this case, τ_2 varies generally from 160 to 1300 s and τ_3 from 4300 to 7000 s (except for an abnormally high and unreliable value for the 40% PEO composition), as compared to predicted values of approximately 10^6 s for τ_R and 10^8 s for τ_d, Fit is therefore not good for any τ values. It must, however, be recalled that these values were obtained with very drastic approximations. Another approach is therefore needed to attempt assignment of τ_2 and τ_3 for PEO.

From Eqs. (5)–(7), the following relationships are expected between τ_e, τ_R and τ_d in the framework of the Doi–Edwards theory:

$$\tau_R/\tau_e = Z^2 \text{ or } Z = \sqrt{\tau_R/\tau_e} \quad (10)$$

and

$$\tau_d/\tau_R = 3Z \quad (11)$$

From the M_w and M_e values of the pure polymers, from Eq. (8), and considering that the molecular weight between entanglements of each polymer in the blends probably lies between that of the pure polymers, a Z value of the order of 1–15 is expected for PVPh, and of 30–400 for PEO. As seen in Table 3, the value obtained for $(\tau_2/\tau_1)^{1/2}$ matches well with the expected Z value for PVPh, thus confirming the assignation of τ_2 to τ_R. The Z value as derived from Eq. (11), $\tau_3/3\tau_2$, also fits, within error estimation by propagation of uncertainties, with Z values obtained by Eq. (10), $(\tau_2/\tau_1)^{1/2}$, which confirms the assignment. On the other hand, the $(\tau_2/\tau_1)^{1/2}$ fit is poor for PEO, but the $(\tau_3/\tau_1)^{1/2}$ values are in the correct range of 16–34, as compared to the expected values of 30–400. On this basis, assignment of τ_3 to τ_R is proposed for PEO, whereas assignment of τ_2 is left open, and may be related to chain end relaxation, as previously proposed in the literature [11].

3.6. Molecular significance of changes in relaxation times

An explanation for the behavior of the experimental relaxation times lies in the combination of four often competing variables: ζ, M_e, N and b. First of all, chain friction is the physical parameter accounting for the difficulty with which chain units diffuse by Brownian motion. Therefore, an increase in chain friction also translates to an increase in relaxation time. The chain friction coefficient is related to interchain interactions, and is therefore expected to vary with the number of hydrogen bonds in the system. A near-FTIR study on this system [22] has previously shown that, although the total number of OH groups involved in hydrogen bonding (including PVPh–PVPh and PVPh–PEO hydrogen bonds) increased up to approximately a 50 wt% PEO composition and remained constant up to a 60 wt% concentration, above which no measurements were performed. This increase is due to the occurrence of interchain PVPh–PEO hydrogen bonds, which decrease the number of free OH groups. Based on these data, the chain friction coefficient should first increase, and then remain constant upon addition of PEO to PVPh. Therefore, chain friction coefficient changes should result in an increase in PVPh relaxation, followed by stabilization, but no decrease is expected, contrary to the experimental behavior at 40 wt% PEO, where relaxation times clearly decrease.

Secondly, the molecular weight between entanglements M_e, which may equivalently also be expressed through Z, has a bivalent impact on chain relaxation. On one side, it defines the size of a "Rouse-like" chain relaxing with a relaxation time τ_e by unit diffusion. Hence, the shorter this chain is, the smaller τ_e becomes. On the other hand, Z represents the number of topical obstacles for a chain engaged in reptation, meaning that it takes longer to complete reptation for more entangled systems. Pure PEO is actually much more entangled than pure PVPh with a M_e of 2200 g mol^{-1} [24] for the former and 29,300 g mol^{-1} for the latter [23]. In the blends, M_e is expected, from models proposed by Wu [35] and Tsenoglou [36,37] not accounting for specific interactions, to vary monotonously with composition.

Consequently, addition of PEO to the blends should result in a decrease of the characteristic relaxation times τ_1, while the opposite is observed. Nonetheless, recalling that ζ is thought to slow relaxation down in the same concentration range, a competing contribution of these two parameters may explain the maximum of τ_1^{PVPh} attained at 35 wt% PEO and the subsequent decrease at 40 wt%.

Although this hypothesis holds for τ_1, retraction should not depend on M_e, and thus the shape of τ_2^{PVPh} has to be explained otherwise. The last two variables at play in relaxation, N and b, are so interwoven that they must be discussed together. These parameters reflect the level of coarse-graining involved in the Rouse statistics. From the scaling laws, $N' = N/\lambda$ (where λ is a simple proportionality constant and N' is the new scaled number of chain units) and $b' = \sqrt{\lambda}\cdot b$ (where b' is the effective length of units forming the new scaled chain) [30]. The full length of the new Rouse chain is equal to $Nb/\sqrt{\lambda}$. As b increases, full chain length decreases and vice versa as illustrated in Fig. 10. Chain rigidity should decrease with addition of PEO and chain tortuosity should become more important, leading to longer relaxation times [4]. Experimental evidence for this change was obtained in the present work by observing changes in the $\alpha(\lambda)$ values, which are usually taken as constant. In the present case, 30% changes were observed, which can be attributed to changes in the length of the Kuhn segments with composition. Thus, the behavior of the

Table 3
Estimations of the Z values using different approaches ($\lambda = 1.5$, $T = T_{gf} + 2$ °C, $M_w^{PEO} = 830{,}000$ g mol^{-1})

	PVPh				PEO			
	PEO 25%	PEO 30%	PEO 35%	PEO 40%	PEO 25%	PEO 30%	PEO 35%	PEO 40%
M_w/M_e – PVPh	1				30			
M_w/M_e – PEO	15				400			
$(\tau_2/\tau_1)^{1/2}$	4 ± 1	4 ± 2	4 ± 1	4 ± 1	5 ± 2	4 ± 1	4 ± 1	6 ± 1
$(\tau_3/\tau_1)^{1/2}$	26 ± 8	18 ± 9	11 ± 1	24 ± 10	34 ± 11	21 ± 7	16 ± 6	–
$\tau_3/3\tau_2$	11 ± 3	7 ± 3	3 ± 1	11 ± 4	15 ± 4	9 ± 2	5 ± 2	–

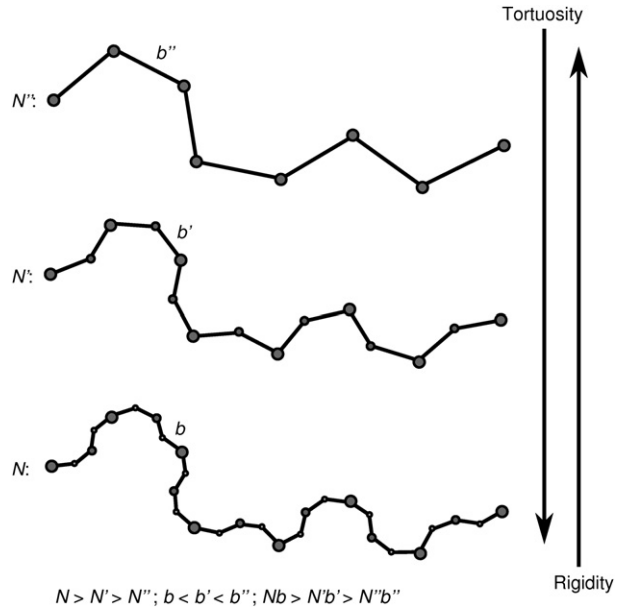

Fig. 10. Schematic representation of the influence of rigidity of the chain on the coarse-graining used in Rouse statistics.

characteristic relaxation times is proposed to spring from simultaneous and competing contributions of the increase in ζ, the variation of M_e and the increase in tortuosity upon incorporation of PEO to PVPh.

For the 30 wt% blend, relaxation measurements were also performed with a different molecular weight PEO (430,000 g mol^{-1} vs 830,000 g mol^{-1}). Relaxation curves recorded for the PEO component of blends with the two different molecular weights appear in Fig. 11. For comparison purposes, the curves obtained for two samples for which M_w was of 830,000 g mol^{-1} are reported along one at 430,000 g mol^{-1}. As can be seen, differences observed between the two curves of the same molecular weight are often greater than those observed for curves using two different weights. There is, within experimental error, no

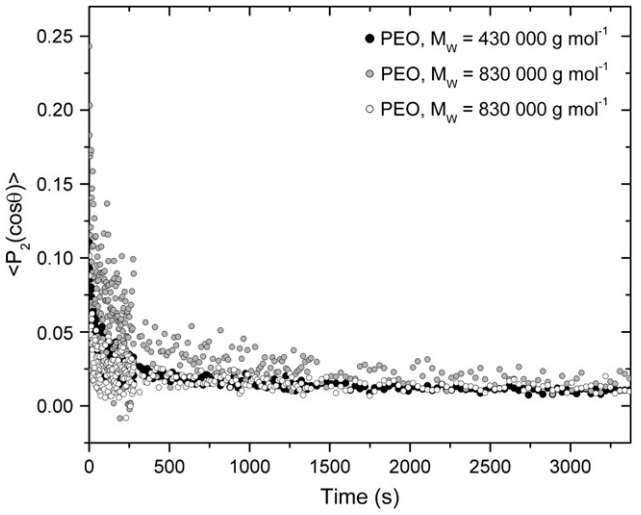

Fig. 11. Relaxation of PEO in a 30 wt% blend for representative samples using two different PEO molecular weights at $T_{gf} + 2$ °C and $\lambda = 1.5$.

clear indication that the molecular weight of PEO influences relaxation under the concentration, temperature and time frame studied here.

3.7. Investigation of relaxation coupling between the two polymers

To gain further insight on the relation of relaxation processes involved in the PEO–PVPh blends, it was interesting to analyze the data in the light of a framework encompassing how one component orientation affects the other.

Tassin and coworkers [38] have proposed, based on an original theory by Doi et al. [39], that orientation coupling can be represented by the following equation:

$$\frac{\langle P_2(cos\,\theta)\rangle_{short}(t)}{\langle P_2(cos\,\theta)\rangle_{long}(t)} = \frac{\varepsilon(1-\varphi_{short})}{1-\varepsilon\varphi_{short}} \tag{12}$$

where ε is the coupling parameter, indicative of the strength of so-called nematic interactions that cause coupling, and φ_{short} the short chain volume fraction. This equation was proposed for short and long chains of the same polymer in which the intrinsic orientation of the short chains is equal to zero. It has been further generalized to extract ε for binary systems where φ_{short} is small [26,40–43].

It was not possible to determine ε for blends in this study because composition revolves around equimolarity and φ_{short} is not precisely known. Yet, it is of interest to assess relaxation cooperativity using $\langle P_2(\cos\theta)\rangle^{PVPh}$ vs $\langle P_2(\cos\theta)\rangle^{PEO}$ plots.

On the basis of the previous equation, a necessary condition for cooperativity in relaxation processes would be that a relation of $\langle P_2(\cos\theta)\rangle^{PVPh}$ with respect to $\langle P_2(\cos\theta)\rangle^{PEO}$ has to be linear (at least at low orientations) and pass through the origin. In other words, the binary system has to return to the isotropic state following the same steps (but not necessarily at the same rate), and should reach $\langle P_2(\cos\theta)\rangle = 0$ at the same time.

Orientation curves of PVPh as a function of PEO orientation are reported in Fig. 12. For the 25 and 30 wt% PEO composition, a linear relationship passing through the origin of the graph is clearly observed. The slopes of 0.48 ± 0.01 and 0.52 ± 0.01 could be used to calculate the interaction parameter ε for 25 and 30 wt% PEO blends, respectively, if φ_{short} was known.

Upon further addition of PEO (for the 35 and 40 wt% PEO), data are linear but the regression line does not pass through the origin. Deviation from this equation can stem from various causes. Firstly, the relaxation time may not be sufficient for 'short' chains to attain an intrinsic orientation value of zero. Secondly, species are not the same, and the hypothesis of identical variables for the tube may not be applicable. But why, for the 25 and 30 wt% compositions, was a single tube parameter sufficient, whereas for higher PEO compositions, two tube parameters would be necessary?

Previous experimental investigations of PVPh–PEO blends [23,44] have shown that molecular weight between entanglements does not follow an athermal rule: For lower PEO compositions, observed values are much higher than those

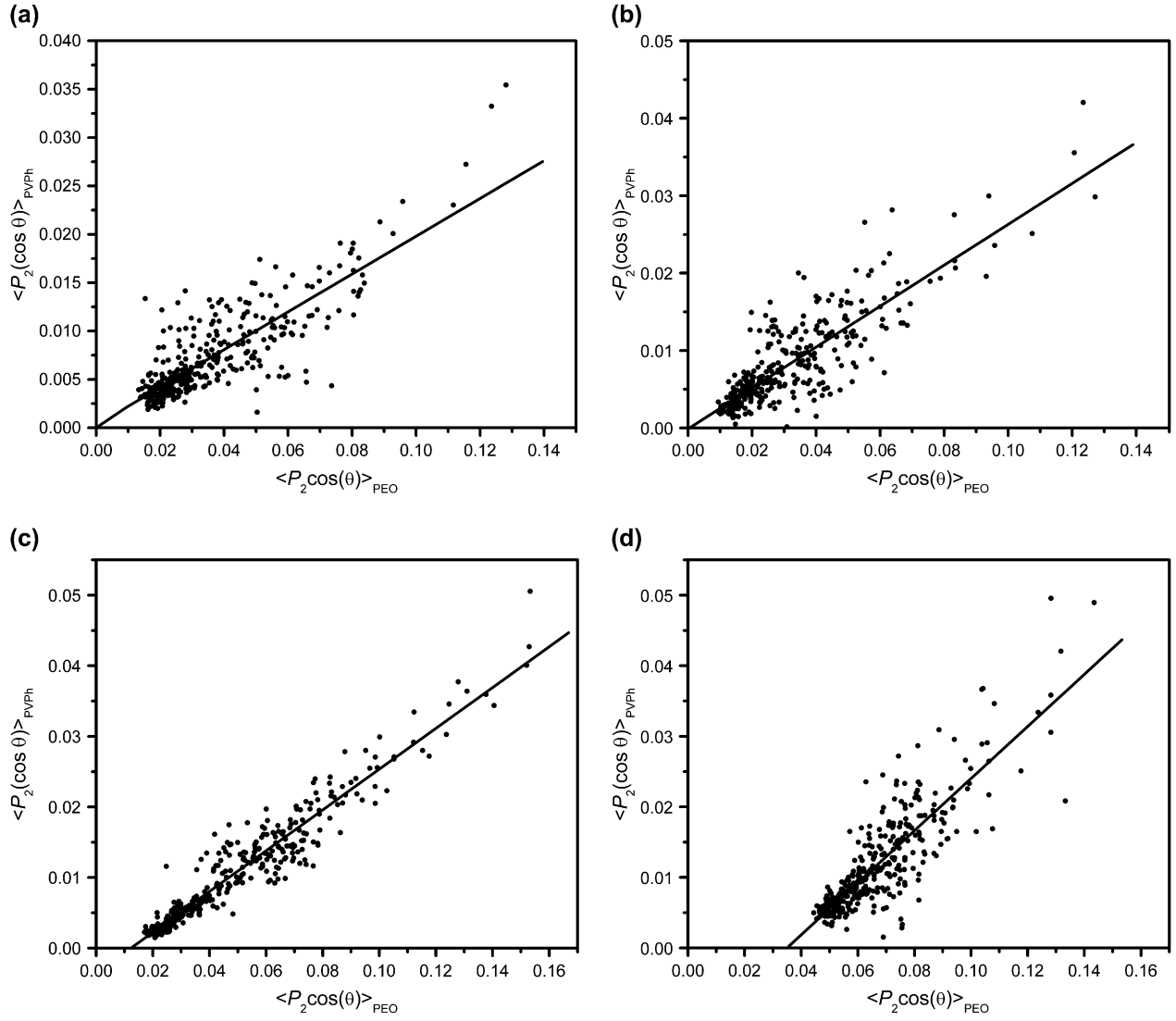

Fig. 12. Relationship between the orientation factor of PEO and PVPh used for the evaluation of relaxation coupling in typical PEO–PVPh blends ($\lambda = 1.5$, $T = T_{gf} + 2\,^{\circ}C$, $M_w^{PEO} = 830{,}000\ g\ mol^{-1}$). (a) PEO 25 wt%, (b) PEO 30 wt%, (c) PEO 35 wt%, (d) PEO 40 wt%.

predicted in these models, but experience a decrease around 35 wt% and revert to the predictions of the athermal model for the 40 wt% PEO composition. This occurs around the same composition at which the first relaxation time of PVPh suddenly decreases. It is therefore proposed that when PVPh forms the dominating network, relaxation cooperativity is due to the fact that PEO is bound to the PVPh network through hydrogen bonds and behaves as the latter.

At higher PEO concentrations, around 30 wt% (or 54 mol%), PEO becomes the dominating network. PVPh does not follow the relaxation of this PEO-based network, and individual Rouse unit lengths are required to explain the observed decrease in relaxation times of PVPh, as discussed in the previous section. In this case, PVPh segments are almost equally hydrogen bonded to the PEO network and to other PVPh segments, as demonstrated by previous near-FTIR measurements [12,22], and thus cannot follow readily the PEO network relaxation.

Therefore, it can be proposed that a necessary condition for cooperativity to occur in a given concentration range is that the minor component of the blend must preferentially interact with the major component. This was true for lower PEO compositions (25 and 30 wt% PEO), where PEO binds to PVPh, but not for higher ones, as the minor PVPh component will equally hydrogen bond to itself and to PEO, and will therefore not preferentially interact with the major component of the blend. The number of interactions between the two polymers insures miscibility at the DSC level, although relaxation cooperativity is lost. To observe cooperativity in the whole composition range, interchain hydrogen bonds would have to be sufficiently favored to compete with intrachain hydrogen bonds.

4. Conclusion

For the PVPh–PEO blends, which form strong hydrogen bonds, the present work shows that an increase in the

relaxation times occurs upon increasing PEO concentration for PEO at all compositions and for PVPh up to 35 wt% PEO. This behavior was attributed to a combination of an increase in the friction coefficient, due to an increase in number of hydrogen bonds, to variations in the chain entanglements and to a gain in chain tortuosity [23].

Although all blend compositions studied present important interchain hydrogen bonding, not all compositions show orientation coupling. Coupling is lost at higher PEO concentration, which is attributed to a change in dominating network. When PVPh dominates, PEO is linked to it and relaxes in a similar way. On the other hand, when PEO is the dominating network, PVPh does not follow the relaxation of the PEO network due to the presence of an important proportion of PVPh–PVPh hydrogen bonds. Conformation and tortuosity are thus modified, which in turn modifies the length and number of segments to be used in Rouse statistics. A decrease in the relaxation time of the PVPh component follows. It is therefore proposed that hydrogen bonds can promote cooperativity in a blend, but only in concentration ranges where the minor constituent interacts predominantly with the major constituent.

Acknowledgements

The authors would like to acknowledge the financial support of NSERC (National Science and Engineering Council of Canada) and the FQRNT (Fonds québécois de la recherche sur la nature et les technologies) of the government of Québec. The help of Rodica Plesu and Serge Groleau, of the CERSIM, is also gratefully acknowledged.

References

[1] Jasse B, Tassin J-F, Monnerie L. Prog Colloid Polym Sci 1993;92:8–22.
[2] de Gennes P-G. J Chem Phys 1971;55:572–9.
[3] Bazuin CG, Fan XD, Lepilleur C, Prud'homme RE. Macromolecules 1995;28:897–903.
[4] Zhao Y, Prud'homme RE, Bazuin CG. Macromolecules 1991;24:1261–8.
[5] Gestoso P, Brisson J. Polymer 2001;42:8415–24.
[6] Rinderknecht S, Brisson J. Macromolecules 1999;32:8509–16.
[7] Li D, Brisson J. Macromolecules 1997;30:8425–32.
[8] Brisson J. Polym Eng Sci 2004;44:241–51.
[9] Buffeteau T, Desbat B, Pézolet M, Turlet JM. J Chim Phys Phys-Chim Biol 1993;90:1467–89.
[10] Buffeteau T, Pézolet M. Appl Spectrosc 1996;50:948–55.
[11] Messé L, Pézolet M, Prud'homme RE. Polymer 2000;42:563–75.
[12] Bokobza L, Buffeteau T, Desbat B. Appl Spectrosc 2000;54:360–5.
[13] Oultache AK, Kong X, Pellerin C, Brisson J, Pézolet M, Prud'homme RE. Polymer 2001;42:9051–8.
[14] Pellerin C, Prud'homme RE, Pézolet M, Weinstock BA, Griffiths PR. Macromolecules 2003;36:4838–43.
[15] Moskala EJ, Varnell DF, Coleman MM. Polymer 1985;26:228–34.
[16] Qin C, Pires ATN, Belfiore LA. Polym Commun 1990;31:177–82.
[17] Zhang X, Takegoshi K, Hikichi K. Macromolecules 1992;25:2336–40.
[18] Jack KS, Whittaker AK. Macromolecules 1997;30:3560–8.
[19] Buffeteau T, Pézolet M. In: Griffiths PR, editor. Linear dichroism in infrared spectroscopy. Handbook of vibrational spectroscopy, vol. 1. Chichester: John Wiley & Sons Ltd; 2002. p. 693–710.
[20] Utracki LA. Adv Polym Technol 1985;5:33–9.
[21] Li D, Brisson J. Polymer 1994;35:2078–83.
[22] Cai H, Brisson J. J Near Infrared Spectrosc 2003;11:183–91.
[23] Cai H, Ait-Kadi A, Brisson JJ. Appl Polym Sci 2004;93:1623–30.
[24] Wu S. J Polym Sci Polym Phys Ed 1989;27:723–41.
[25] Duchesne C, Kong X, Brisson J, Pézolet M, Prud'homme RE. Macromolecules 2002;35:8768–73.
[26] Messé L, Prud'homme RE. J Polym Sci Polym Phys Ed 2000;38:1405–15.
[27] Pellerin C, Prud'homme RE, Pézolet M. Macromolecules 2000;33:7009–15.
[28] Tassin J-F, Monnerie L. Macromolecules 1988;21:1846–54.
[29] Thirion P, Tassin JF. J Polym Sci Polym Phys Ed 1983;21(10):2097–108.
[30] Doi M, Edwards SF. The theory of polymer dynamics. Oxford, New York: Clarendon Press, Oxford University Press; 1986.
[31] Takahashi Y, Sumita I, Tadokoro H. J Polym Sci Polym Phys Ed 1973;11(11):2113–22.
[32] Brandrup J, Immergut EH, Grulke EA. Polymer handbook. 4th ed. New York, Toronto: John Wiley & Sons; 1999.
[33] Dong H, Hyun J-K, Durham C, Wheeler RA. Polymer 2001;42:7809–17.
[34] Kawaguchi S, Imai G, Suzuki J, Miyahara A, Kitano T, Ito K. Polymer 1997;38:2885–91.
[35] Wu S. J Polym Sci B Polym Phys 1987;25:2511–29.
[36] Tsenoglou C. J Polym Sci B Polym Phys 1988;26:2329–39.
[37] Tsenoglou C. Macromolecules 1991;24:1762–7.
[38] Tassin J-F, Baschwitz A, Moise JY, Monnerie L. Macromolecules 1990;23:1879–81.
[39] Doi M, Pearson D, Kornfield J, Fuller G. Macromolecules 1989;22:1488–90.
[40] Saito H, Miyashita H, Inoue T. Macromolecules 1992;25:1824–7.
[41] Saito H, Takahashi M, Inoue T. J Polym Sci B Polym Phys 1988;26:1761–8.
[42] Kawabata K, Fukuda T, Tsujii Y, Miyamoto T. Macromolecules 1993;26:3980–5.
[43] Fukuda T, Kawabata K, Tsujii Y, Miyamoto T. Macromolecules 1992;25:2196–9.
[44] Cai H, Ait-Kadi A, Brisson J. Polymer 2003;44:1481–9.